Magnetization splitting in Landau and diamond-domain structures: Dependence on exchange interaction, anisotropy, and size

Kaixuan Xie,[1] Xiaopu Zhang,[1] Weiwei Lin,[2,*] Peng Zhang,[1] and Hai Sang[1,*]
[1]*National Laboratory of Solid State Microstructures, School of Physics, Nanjing University, Nanjing 210093, China*
[2]*Institut d'Electronique Fondamentale, Université Paris-Sud, Orsay 91405, France*
(Received 16 April 2011; revised manuscript received 11 June 2011; published 17 August 2011)

The distributions of magnetization orientation for both Landau and diamond-domain structures in nanorectangles have been investigated by micromagnetic simulation. Both symmetric and asymmetric magnetization splitting are found in the diamond-domain structure, as well as only symmetric magnetization splitting in the Landau structure. The magnetization splitting can take place around both the easy axis and the hard one. These indicate that the magnetization splitting is a *general* behavior in both Landau and diamond-domain structures. In the Landau structure, the splitting angle increases with the exchange coefficient but decreases slightly with the anisotropy constant, suggesting that the exchange interaction mainly contributes to the magnetization splitting in Landau structure. However in the diamond structure, the splitting angle increases with the anisotropy constant but decreases with the exchange coefficient, indicating that the magnetization splitting in the diamond structure mainly results from magnetic anisotropy. For both Landau and diamond-domain structures, the magnetization splitting depends strongly on the size. In the case of the easy axis along the length direction, the magnetization splitting angle around the easy axis is enhanced with the length of the easy axis, while that around the hard axis increases with the length of the hard axis. These results can extend the understanding of the basic features of the magnetic domain microstructures.

DOI: 10.1103/PhysRevB.84.054460 PACS number(s): 75.60.Ch, 75.30.Et, 75.75.−c, 75.78.Cd

I. INTRODUCTION

Magnetic nanostructures are actively studied, not only for their high-sensitivity function[1] or excitations of magnetic moments for practical application,[2,3] but also as good candidates in research on some fundamental and interesting aspects of magnetism in physics.[4–8] Their domain structures and magnetic properties are strongly related with a few intrinsic parameters, such as magnetization, exchange coefficient, and the anisotropy constant.[9] Moreover, the size,[10–13] the aspect ratio,[14,15] and the thickness[5,7,12,15] of the magnetic nanostructure have a dramatic impact on the magnetic properties,[16–19] especially when the size is comparable to the exchange length.[9]

The framework of micromagnetic simulation can describe the magnetization configuration and dynamics in a scale between several tens of nanometers and a few microns.[4,5,20] Basically, there are two ways to view micromagnetic calculations. One is based on the integration of the equation, which is the motion of the magnetic moments described by the Landau-Lifshitz-Gilbert (LLG) equation. The other is to minimize the total magnetic energy. The former prefers the time-dependent evolution of magnetization,[21] while the latter is in a perspective of energy. In order to reduce the exchange energy, a uniform magnetization is ideal, but the demagnetization energy would like magnetization parallel to the surface or poles counterbalanced at the interface. Meanwhile, the magnetic moment favors low anisotropy energy if its magnetization is along the easy direction. Without the external magnetic field, the magnetization will relax to an equilibrium state, which is the competition among these three energy items and reach a local minimum energy. No matter what the spatial dimension differences[12–15,22] or roughness variety,[4,23,24] from a viewpoint of minimum energy, they all act on the local and nonlocal magnetic energy items.[9]

In thin soft elements, the Landau state and the diamond state are well known as typical magnetic flux-closure patterns and prominent candidates of magnetic ground state.[4,5,15] The magnetization orientation splitting has been observed in the flux-closure domain in Ref. 4, which means the majority of the magnetizaton orientation in the splitting domain is slightly away from the axis within the plane of the rectangle, and its roughness dependence has been explained successfully by micromagnetic simulation. The magnetization splitting is a basic and important feature of the magnetic domain microstructures. However up to now, the magnetization splitting was only reported in the Landau structure, and it is symmetric.[4] It is interesting to check this behavior also in the diamond-domain structure. More important, the origin of the magnetization splitting is still unclear. It is needed to study the dependence of the magnetization splitting on some intrinsic parameters such as exchange interaction, magnetic anisotropy, and size.

In this work, we investigate the distributions of magnetization orientation for both Landau and diamond-domain structures in nanorectangles by micromagnetic simulation. Besides symmetric magnetization splitting in the Landau domain structure, both symmetric and asymmetric magnetization splitting are found in the diamond structure. The magnetization splitting can take place around both the easy axis and the hard one. These indicate that the magnetization splitting is a *general* behavior in both Landau and diamond-domain structures. From the dependence of the splitting angle on the exchange coefficient and the anisotropy constant, it suggests that the exchange interaction mainly contributes to the magnetization splitting in the Landau structure, while that in the diamond structure is dominated by magnetic anisotropy. For both the Landau and diamond-domain structures, the magnetization splitting depends strongly on the size. In the case of the easy axis along the length direction, the magnetization splitting

angle around the easy axis is enhanced with the length of the easy axis, while that around the hard axis increases with the length of the hard axis.

The paper is organized as follows. Section II describes the micromagnetic simulation model and method. Section III shows the magnetic anisotropy dependence of the magnetization distribution and splitting in Laudau and diamond-domain structures. Their dependence on the exchange interaction and size is discussed in Secs. IV and V, respectively.

II. SIMULATION METHOD

We made a systematic investigation on the magnetization orientation splitting in both Landau and diamond-domain structures in nanorectangles by micromagnetic simulation with the Object Oriented Micromagnetic Framework (OOMMF), based on a model of Standard Problem 1.[25] The dependence of magnetization splitting on the exchange coefficient and anisotropy constant was studied. The principle of minimum energy and the symmetry of magnetic microstructure[23,26] were employed to explain the different dependence and distribution features. The simulated rectangle size is 1000 × 500 × 20 nm^3 in Secs. III and IV, while in Sec. V, the lateral size is varied to show the dimension dependence. In every rectangle, the cell size is no larger than 5 × 5 × 5 nm^3, and the cell number is no less than 80 000 cells, which could meet the requirement of both simulations and the following statistic. In our simulation, no external magnetic field was applied. The total energy E includes the exchange energy E_{ex}, anisotropy energy E_A, and demagnetizing energy E_D, where

$$E_{ex} = \int_{(V)} A[(\nabla m_x)^2 + (\nabla m_y)^2 + (\nabla m_z)^2]dV, \quad (1)$$

$$E_A = \int_{(V)} K\left(\alpha_1^2\alpha_2^2 + \alpha_1^2\alpha_3^2 + \alpha_2^2\alpha_3^2\right) dV, \quad (2)$$

$$E_D = -\frac{\mu_0}{2}\int_{(V)} \boldsymbol{M} \bullet \boldsymbol{H}_d dV. \quad (3)$$

In the simulation, the minimization of total energy is performed by using the conjugate gradient method with no preconditioning,[27,28] by locating the local minimum in the energy surface. The parameters of permalloy are used here as reference. The saturation magnetization M_S is 8.6 × 10^5 A/m, the exchange coefficient A between cells varies from 9 × 10^{-12} J/m to 2.3 × 10^{-11} J/m, and the anisotropy constant K is between −900 J/m^3 and 900 J/m^3, respectively. Different magnetization configurations are chosen as the initial state without considering the thermal activation. Then, it converges in a minimum energy state confined by the local energy barrier.[15] For an initial magnetization state described in Fig. 1(a), it relaxes into the Landau state as shown in Fig. 1(c); while a diamond state will form in the case of an initial state in Fig. 1(b), as shown in Fig. 1(d). The up direction of the short axis (Y) of the rectangle is defined as 0° direction. The positive anisotropy constant K means the magnetizaton prefers 90° or 270°, i.e., the long axis (X). Either the diamond structure or the Landau structure is converged to, although the total energy of each differs for different A and K. The dependence of the total energy on A and K is shown in Figs. 1(e) and 1(f),

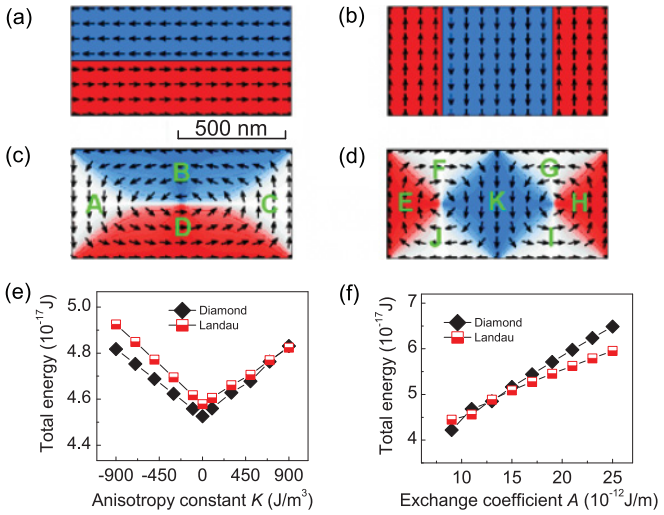

FIG. 1. (Color online) (a) and (b) Two initial magnetization states for relaxing into the Landau domain structure (c) and diamond-domain structure (d), respectively. Blue and red represent two opposite magnetization orientations, and the arrows show the directions of magnetization. (e) Dependence of total energy on the anisotropy constant K. (f) Dependence of total energy on the exchange coefficient A.

respectively. It is found that mostly the lower total energy prefers the diamond structure as K changes. This is similar to the results in the literature.[13] However, the lower energy favors the Landau structure as A larger than 1.5 × 10^{-11} J/m.

III. MAGNETIC ANISOTROPY DEPENDENCE

Figure 2(a) shows a typical distribution curve of magnetization orientation as a function of the magnetization angle θ in the Landau domain structure. The proportion density $\varphi(\theta)$ describes the relative frequency for a given θ. The proportion of the magnetization within a particular range of angle is given by the integral of proportion density $\varphi(\theta)$ over this range. The area under distribution curve from 0° to 360° equals 100%. The $\varphi(\theta)$ is calculated as the count in a step of 1.2° over the product of total cell amount and the step. The distribution curve of magnetization orientation shows a minimal period of 180°, corresponding to the centrosymmetry in the Landau domain structure. Four main peaks P_1, P_2, P_3, and P_4 correspond to four different magnetization orientations in domain C, B, A, and D, respectively, in Fig. 1(c). P_2 (P_4) splits into two symmetric peaks P_{2L} and P_{2R} (P_{4L} and P_{4R}) with a valley V_2 (V_4), which corresponds to the magnetization orientations in domain B (D) aligning around the long edges.[4] V_{23} is the valley between P_2 and P_3, which is located in the 90° domain wall between domain A and B. Hereafter, we name all the peaks and valleys in this way. Figure 2(b) shows the distribution curves of P_1 for $K = -900$, 0 and 900 J/m^3, in the case of $A = 1.3 \times 10^{-11}$ J/m, and those of P_2 are shown in Fig. 2(c). The splitting angle $\Delta\theta$ between P_{2L} and P_{2R} defined by the half depth of the valley is about 9.2° [see Fig. 2(c)]. The φ of P_1 decreases as K increases, while those of P_{2L}, P_{2R}, and V_2 increase with K, as shown in Fig. 2(d). It indicates that there is a net increment of magnetization in domain B but a decrement of that in domain C. More

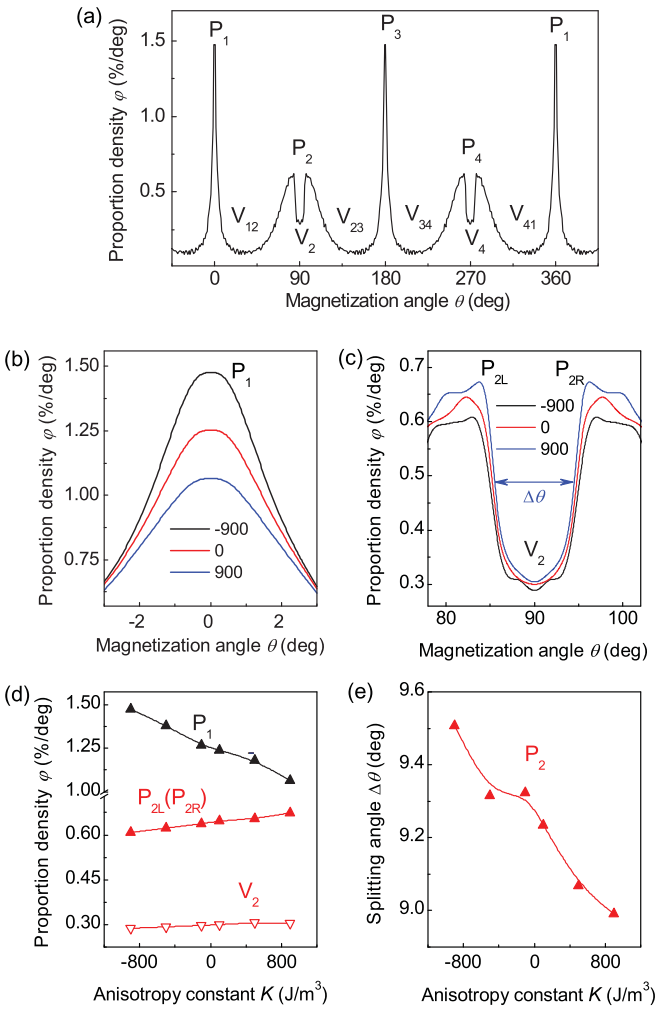

FIG. 2. (Color online) For the Landau structure: (a) the distribution curve of magnetization orientation as a function of the magnetization angle θ. (b) The distribution curves of P_1 for $K = -900$, 0 and 900 J/m^3, as $A = 1.3 \times 10^{-11}$ J/m. (c) The distribution curves of P_2 for $K = -900$, 0 and 900 J/m^3, as $A = 1.3 \times 10^{-11}$ J/m. (d) Dependence of the proportion densities φ on K for P_1, P_2, and V_2. (e) Dependence of the splitting angle $\Delta\theta$ on K for P_2.

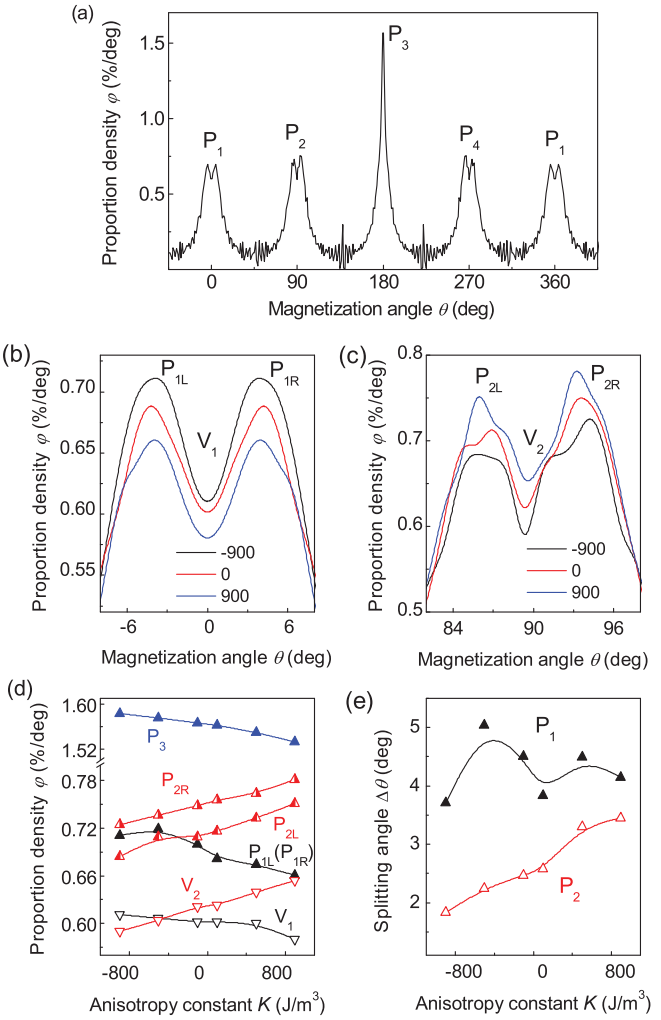

FIG. 3. (Color online) For the diamond structure: (a) the distribution curve of magnetization orientation as a function of the magnetization angle θ. (b) The distribution curves of P_1 for $K = -900$, 0 and 900 J/m^3, as $A = 1.3 \times 10^{-11}$ J/m. (c) The distribution curves of P_2 for $K = -900$, 0 and 900 J/m^3, as $A = 1.3 \times 10^{-11}$ J/m. (d) Dependence of the proportion densities φ on K for peaks and valleys. (e) Dependence of $\Delta\theta$ on K for P_1 and P_2.

magnetization aligns close to the easy axis for benefiting a low total energy when the anisotropy constant K is larger. It can be seen from Fig. 2(e) that the splitting angle $\Delta\theta$ of P_2 decreases slightly as K increases, indicating that the anisotropy has weak influence on the splitting angle in the Landau structure.[4]

For the diamond-domain structure, a typical distribution curve of magnetization orientation is shown in Fig. 3(a) as a function of the magnetization angle θ. The distribution curve exhibits four main peaks P_1, P_2, P_3, and P_4 in a period of 360°, which shows mirror symmetry with the short axis in the diamond structure [see Fig. 1(d)]. It is interesting that the magnetization splitting can be found in P_1, P_2, and P_4. As shown in Fig. 3(b), P_1 splits into two symmetric peaks P_{1L} and P_{1R}, corresponding to the magnetization orientation in domains E and H in Fig. 1(d). However, P_2, whose magnetization around the 90° axis, splits into two asymmetric peaks P_{2L} and P_{2R}, as shown in Fig. 3(c). This asymmetry of the splitting could be induced by the different magnetization characters in neighbors of domains G (J).

It can be seen from Fig. 3(d) that φ of P_{1L} (P_{1R}), V_1, and P_3 decreases as the anisotropy constant K increases. However, φ of P_{2L}, P_{2R}, and V_2 increases with K. This is due to the conservation of the total magnetization in the domain, i.e., wherever the magnetization of P_1 and P_3 gain, there must be partly a loss in that of P_2 and P_4. More magnetization favors aligning around the long axis as K increases. The splitting angle $\Delta\theta$ of P_1 varies a little bit with K, as shown in Fig. 3(e), while that of P_2 increases with K.

IV. EXCHANGE INTERACTION DEPENDENCE

The dependence of magnetization distribution on exchange coefficient A for the Landau structure is shown in Fig. 4, as $K = 500$ J/m^3. The low proportion density φ in V_{12} for the small A [see Fig. 4(b)] means that a sharp domain wall

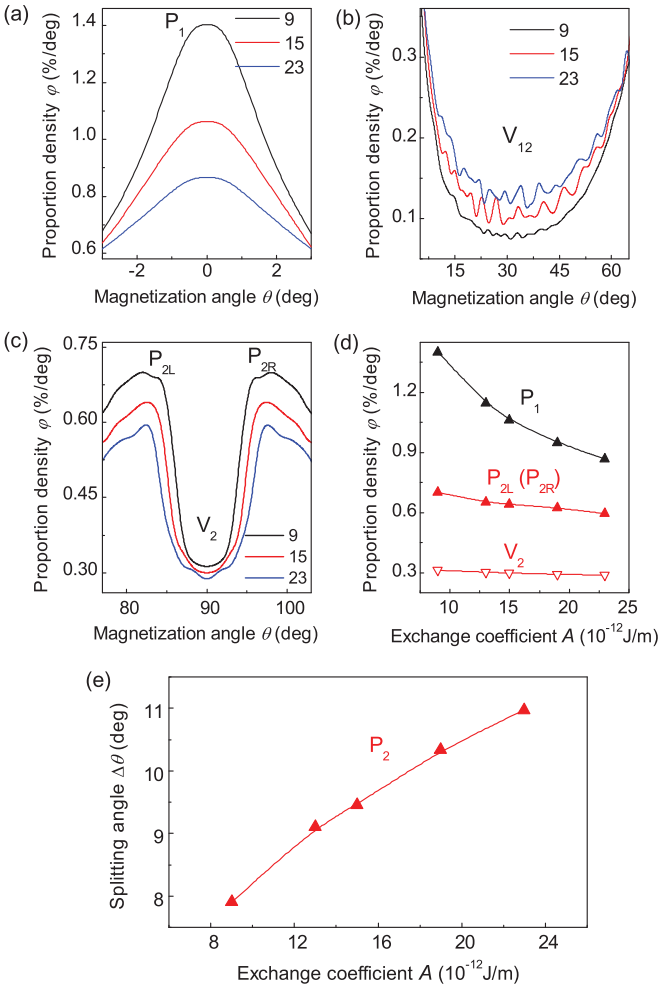

FIG. 4. (Color online) For the Landau structure, the distribution curves of P_1 (a), V_{12} (b), and P_2 (c) for $A = 9 \times 10^{-12}$, 15×10^{-12}, and 23×10^{-12} J/m, as $K = 500$ J/m^3. (d) Dependence of the proportion densities φ on A for P_1, P_2, and V_2. (e) Dependence of $\Delta\theta$ on A for P_2.

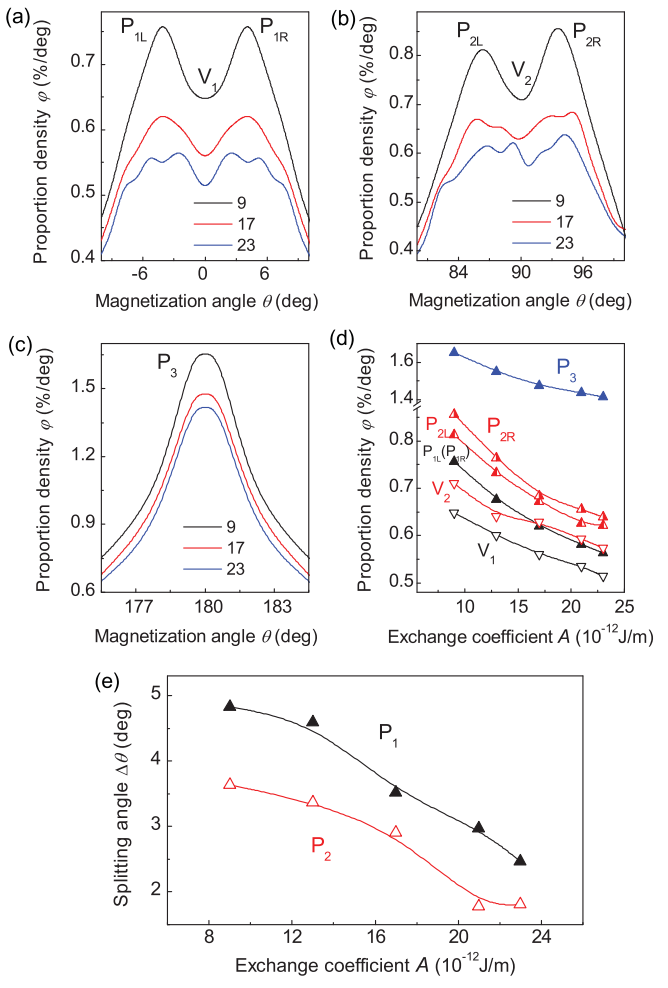

FIG. 5. (Color online) For the diamond structure, the distribution curves of P_1 (a), P_2 (b), and P_3 (c) for $A = 9 \times 10^{-12}$, 17×10^{-12}, and 23×10^{-12} J/m, as $K = 500$ J/m^3. (d) Dependence of the proportion densities φ on A for peaks and valleys. (e) Dependence of $\Delta\theta$ on A for P_1 and P_2.

with small net magnetization is formed between domain B and C, because the small A allows the large angle between neighbor magnetizations for forming the 90° domain wall. This is consistent with the variation of P_1 and P_2 shown in Figs. 4(a) and 4(c), respectively. The φ of P_1, P_{2L} (P_{2R}), and V_2 all increase with the decrease of A as shown in Fig. 4(d). It can be seen from Fig. 4(e) that the splitting angle $\Delta\theta$ of P_2 increases from 7.9° to 11.0° with A from 9×10^{-12} J/m to 2.3×10^{-11} J/m, indicating much more influence than the anisotropy constant. It suggests the exchange interaction mainly contributes to the magnetization splitting in the Landau structure.

For the diamond structure, the magnetization distribution curves of P_1, P_2, and P_3 for the various exchange coefficients A are plotted in Figs. 5(a)–5(c). The φ of P_1, P_2, and P_3 decreases with increasing A, as shown in Fig. 5(d). As the exchange coefficient increases, sharp direction changes of the neighboring magnetic moment are not allowed in the 90° domain wall region. This consumes the domains at both sides of the domain wall and reduces the net magnetization in the domains. It can be seen from Fig. 5(e), $\Delta\theta$ for both P_1 and P_2 decrease with increasing A. This may be due to the change of volume charges created by the two vortices in the middle[4] and the decrease of the net magnetization in every domain as A increases. Due to the fact that the splitting angle $\Delta\theta$ decreases with increasing the exchange coefficient but increases with the anisotropy constant, we suggest that the magnetization splitting in the diamond structure mainly results from magnetic anisotropy.

V. SIZE DEPENDENCE

Next, we show the magnetization splitting in both the Landau and diamond-domain structures with various lateral sizes. Both the length X and the width Y were varied in the rectangles with 20-nm thickness, as $A = 1.3 \times 10^{-11}$ J/m and $K = 500$ J/m^3.

Figures 6(a)–6(d) show the magnetization distribution in the Landau structure in the rectangles with X from 500 nm to 1500 nm and $Y = 500$ nm. The magnetization distribution

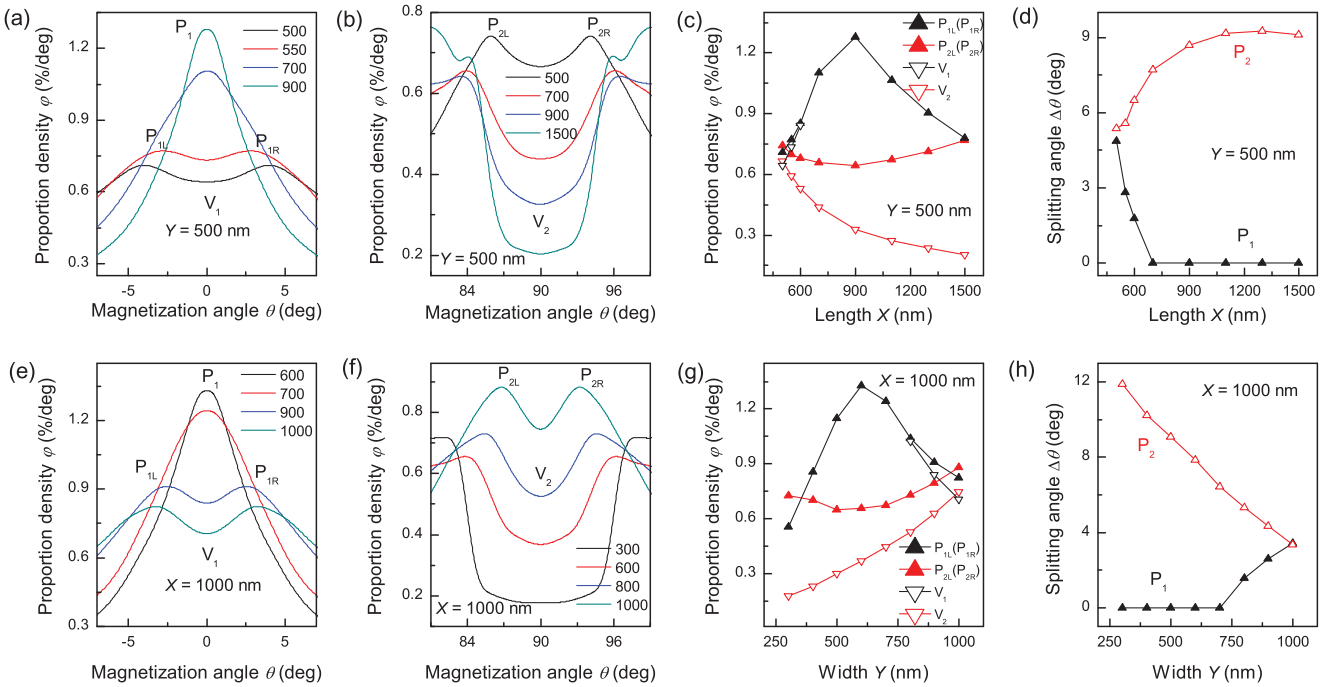

FIG. 6. (Color online) For the Landau structure, the distribution curves of P_1 (a) and P_2 (b) for various X, as $Y = 500$ nm. The units in the legends are nanometers. (c) Dependence of the proportion density φ on X for peaks and valleys. (d) Dependence of $\Delta\theta$ on X for P_1 and P_2. The distribution curves of P_1 (e) and P_2 (f) for various Y, as $X = 1000$ nm. (g) Dependence of φ on Y for peaks and valleys. (h) Dependence of $\Delta\theta$ on Y for P_1 and P_2 ($A = 1.3 \times 10^{-11}$ J/m and $K = 500$ J/m^3).

curve of the peak P_1 around the hard axis (0°) splits into two symmetric peaks P_{1L} and P_{1R} with a valley V_1 for $X = 500$ and 550 nm, as shown in Fig. 6(a), but no splitting for $X = 700$ and 900 nm. However, the distribution curves around the easy axis (90°), shown in Fig. 6(b), exhibit splitting for 500 nm $\leqslant X \leqslant$ 1500 nm. The proportion densities φ of peaks and

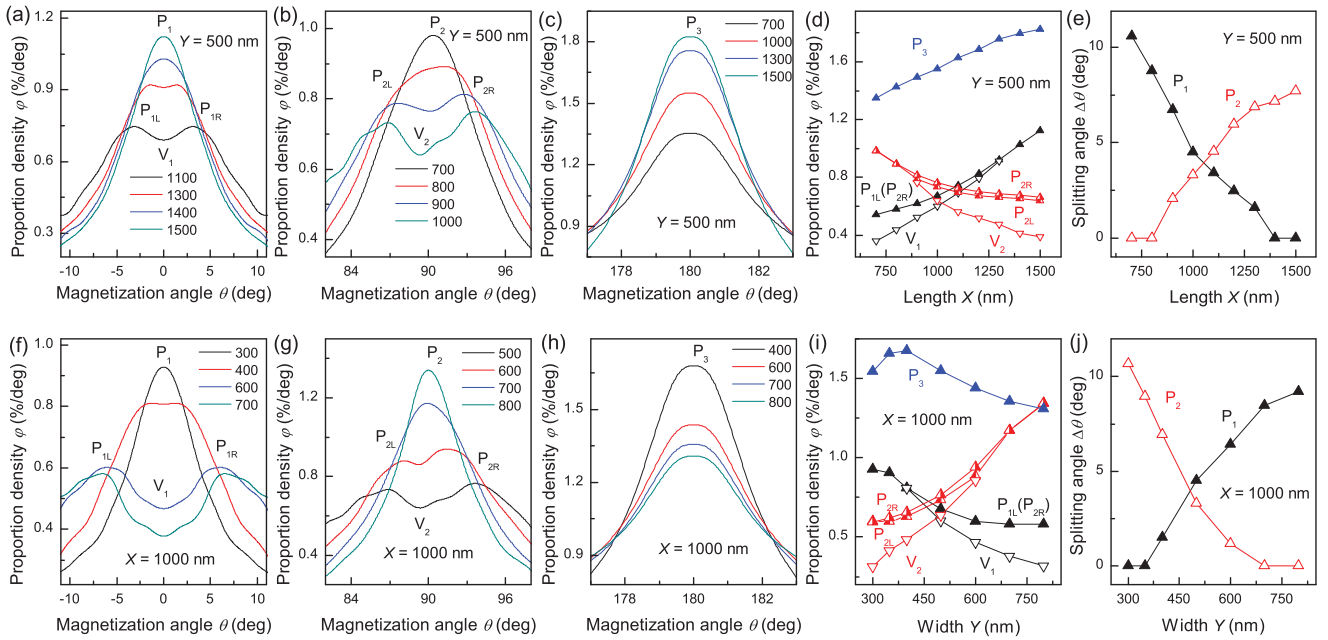

FIG. 7. (Color online) For the diamond structure, the distribution curves of P_1 (a), P_2 (b), and P_3 (c) for various X, as $Y = 500$ nm. The units in the legends are nanometers. (d) Dependence of the proportion density φ on X for peaks and valleys. (e) Dependence of $\Delta\theta$ on X for P_1 and P_2. The distribution curves of P_1 (f), P_2 (g), and P_3 (h) for various Y, as $X = 1000$ nm. (i) Dependence of φ on Y for peaks and valleys. (j) Dependence of $\Delta\theta$ on Y for P_1 and P_2 ($A = 1.3 \times 10^{-11}$ J/m and $K = 500$ J/m^3).

valleys are plotted as a function of X in Fig. 6(c). For $Y =$ 500 nm, with X increasing, the φ of P_1 (P_{1L} and P_{1R} as $X \leqslant$ 600 nm) increases and then decreases, while that of V_1 ($X \leqslant$ 600 nm) increases. However, the trend of P_2 (around the easy axis) is opposite to that of P_1 (around the hard axis). With the increase of X, the φ of P_2 decreases and then increases, while that of V_2 decreases. Figure 6(d) shows the magnetization splitting angles $\Delta\theta$ for P_1 and P_2 as a function of X. With X increasing, $\Delta\theta$ for P_1 (around the hard axis) decreases and becomes zero as $X \geqslant 700$ nm. Nevertheless, $\Delta\theta$ for P_2 (around the easy axis) increases with X.

Figures 6(e) and 6(f) show the corresponding dependence on Y in the range of 300 to 1000 nm as $X = 1000$ nm. As shown in Fig. 6(e), the distribution curves of P_1 around the hard axis does not split for $Y = 600$ and 700 nm but split into two symmetric peaks for $Y = 900$ and 1000 nm. The magnetization splitting for P_2 around the easy axis can be seen in Fig. 6(f) for various Y. The φ of peaks and valleys are plotted as a function of Y in Fig. 6(g). For $X = 1000$ nm, with increasing Y, the φ of P_1 (P_{1L} and P_{1R} as $Y \geqslant 800$ nm) increases and then decreases, however, that of P_2 decreases and then increases. The φ of V_1 ($Y \geqslant 800$ nm) decreases with Y increasing, while that of V_2 increases, which is opposite to the dependence on X. Figure 6(h) shows that $\Delta\theta$ for P_1 becomes nonzero as $Y \geqslant 800$ nm and increases with Y, however, $\Delta\theta$ for P_2 decreases with the increase of Y.

It suggests that for the Landau structure, in the case of the easy axis along the length direction, a large X could inhibit the splitting in P_1 around the hard axis but promotes that in P_2 around the easy axis. In contrast, a large Y could promote the splitting in P_1 but weaken that in P_2. The critical X of splitting around the hard axis is about 700 nm as $Y =$ 500 nm, and the critical Y of splitting is about 700 nm as $X = 1000$ nm. It is noticed that the magnetization splitting around the hard axis takes place as the aspect ratio X/Y is less than 1.4.

For the diamond-domain structure, the proportion density φ and splitting angle $\Delta\theta$ dependence on X and Y are shown in Fig. 7. Figures 7(a)–7(e) describe the rectangles with X between 700 to 1500 nm and $Y = 500$ nm. See Figs. 7(a)–7(c), as X increases, a splitting to nonsplitting transition happens to P_1 (around the hard axis); for P_2 (around the easy axis), while X decreases, P_{2L} and P_{2R} inherit their own asymmetry, collapse, and transfer to an asymmetry nonsplitting peak; P_3 always increases with X. The φ dependence on X is shown in Fig. 7(d). With X increasing from 700 to 1500 nm, P_1, V_1, and P_3 (around the hard axis) increase, but P_2 and V_2 (around the easy axis) decrease. Furthermore, V_1 vanishes, as X is more than 1300 nm, which means no splitting there; V_2 disappears as X is smaller than 900 nm, meaning without splitting. The splitting to nonsplitting transition can also be confirmed by Fig. 7(e), where the $\Delta\theta$ becomes zero for the corresponding X. It also shows clearly that the $\Delta\theta$ of P_1 decreases with increasing X, and P_2 increases with X.

Figures 7(f)–7(j) display the corresponding splitting dependence on Y in the range of 300 to 800 nm as $X = 1000$ nm. It is obvious that in Figs. 7(f) and 7(g), the splitting to nonsplitting transition still exists but with an opposite trend to that in Figs. 7(a) and 7(b). Figure 7(h) displays distribution curves of P_3 for $Y =$ 400, 600, 700, and 800 nm. As shown in Fig. 7(i), with the increase of Y, P_1, V_1, and P_3 (around the hard axis) mainly decrease, but P_2 and V_2 (around the easy axis) increases. Moreover, V_1 disappears as Y is less than 400 nm, corresponding to a symmetry nonsplitting peak there; V_2 disappears when Y is more than 600 nm, which means splitting vanishes and an asymmetrical nonsplitting peak is formed. Figure 7(j) confirms those splitting to nonsplitting transitions with inflection points at $Y = 350$ and 700 nm with a zero splitting angle. The $\Delta\theta$ of P_1 increases with Y, but that of P_2 decreases. It is noted that the Y dependence on $\Delta\theta$ of P_1 and P_2 shows the opposite behavior to the X dependence. It is noticed that the magnetization splitting around the hard axis takes place as the aspect ratio X/Y is less than 2.8, while that around the easy axis takes place as X/Y is more than 1.5.

It suggests that in the diamond structure, as the easy axis along the length direction, a large X could inhibit the splitting in P_1 (around the hard axis) but promotes that in P_2 (around the easy axis). In contrast, a large Y could promote the splitting in P_1 but weaken that in P_2. These behaviors are similar to those in the Landau structure.

VI. CONCLUSIONS

In summary, we have investigated the distributions of magnetization orientation for both Landau and diamond-domain structures in nanorectangles by micromagnetic simulation. Both symmetric and asymmetric magnetization splitting are found in the diamond-domain structure, as well as only symmetric magnetization splitting in the Landau structure. The magnetization splitting can take place around both the easy axis and the hard one. These indicate that the magnetization splitting is a *general* behavior in both Landau and diamond-domain structures. In the Landau structure, the splitting angle $\Delta\theta$ increases with the exchange coefficient A but decreases slightly with the anisotropy constant K, suggesting that the exchange interaction mainly contributes to the magnetization splitting in the Landau structure. However in the diamond structure, the splitting angle $\Delta\theta$ increases with the anisotropy constant K but decreases with the exchange coefficient A, indicating that the magnetization splitting in the diamond structure mainly results from magnetic anisotropy. For both Landau and diamond-domain structures, the magnetization splitting depends strongly on the size. In the case of the easy axis along the length direction, the magnetization splitting angle $\Delta\theta$ around the easy axis is enhanced with the length of the easy axis, while that around the hard axis increases with the length of the hard axis.

Our results can extend the understanding of the basic features of the magnetic domain microstructures and provide possible explanations to the origin of magnetization splitting. We expect the magnetization splitting in the diamond-domain structure could be observed in a future experiment.

ACKNOWLEDGMENTS

This work was partly supported by CSKPOFR Grants No. 2009CB929503 and NSFC No. 20833002.

*Corresponding authors: weiwei.lin@u-psud.fr and haisang@nju.edu.cn

[1] A. Lyberatos, G. Ju, R. J. M. van de Veerdonk, and D. Weller, J. Appl. Phys. **91**, 2236 (2002).
[2] A. Krasyuk, F. Wegelin, S. A. Nepijko, H. J. Elmers, G. Schönhense, M. Bolte, and C. M. Schneider, Phys. Rev. Lett. **95**, 207201 (2005).
[3] J. P. Park, P. Eames, D. M. Engebretson, J. Berezovsky, and P. A. Crowell, Phys. Rev. B **67**, 020403(R) (2003).
[4] S. Hankemeier, R. Frömter, N. Mikuszeit, D. Stickler, H. Stillrich, S. Pütter, E. Y. Vedmedenko, and H. P. Oepen, Phys. Rev. Lett. **103**, 147204 (2009).
[5] R. Hertel, O. Fruchart, S. Cherifi, P.-O. Jubert, S. Heun, A. Locatelli, and J. Kirschner, Phys. Rev. B **72**, 214409 (2005).
[6] H. Kronmüller and R. Hertel, J. Magn. Magn. Mater. **215–216**, 11 (2000).
[7] M. Bode, A. Wachowiak, J. Wiebe, A. Kubetzka, M. Morgenstern, and R. Wiesendanger, Appl. Phys. Lett. **84**, 948 (2004).
[8] A. Kobs, H. Spahr, D. Stickler, S. Hankemeier, R. Frömter, and H. P. Oepen, Phys. Rev. B **80**, 134415 (2009).
[9] A. Hubert and R. Schäfer, *Magnetic Domains: The Analysis of Magnetic Microstructures* (Springer-Verlag, Berlin, 1998), pp. 337–338.
[10] A. Yamasaki, W. Wulfhekel, R. Hertel, S. Suga, and J. Kirschner, Phys. Rev. Lett. **91**, 127201 (2003).
[11] N. A. Usov, C. R. Chang, and Z. H. Wei, J. Appl. Phys. **89**, 7591 (2001).
[12] J. K. Ha, R. Hertel, and J. Kirschner, Phys. Rev. B **67**, 224432 (2003).
[13] W. Rave and A. Hubert, IEEE Trans. Magn. **36**, 3886 (2000).
[14] A. Krasyuk, S. A. Nepijko, A. Oelsner, C. M. Schneider, H. J. Elmers, and G. Schönhense, Appl. Phys. A **88**, 793 (2007).
[15] S. Cherifi, R. Hertel, J. Kirschner, H. Wang, R. Belkhou, A. Locatelli, S. Heun, A. Pavlovska, and E. Bauer, J. Appl. Phys. **98**, 043901 (2005).
[16] J. I. Martín, J. Nogués, K. Liu, J. L. Vicent, and I. K. Schuller, J. Magn. Magn. Mater. **256**, 449 (2003).
[17] R. P. Cowburn, D. K. Koltsov, A. O. Adeyeye, M. E. Welland, and D. M. Tricker, Phys. Rev. Lett. **83**, 1042 (1999).
[18] K. J. Kirk, J. N. Chapman, and C. D. W. Wilkinson, Appl. Phys. Lett. **71**, 539 (1997).
[19] R. D. Gomez, T. Luu, A. Pak, I. Mayergoyz, K. Kirk, and J. Chapman, J. Appl. Phys. **85**, 4598 (1999).
[20] K. Yu. Guslienko, W. Scholz, R. W. Chantrell, and V. Novosad, Phys. Rev. B **71**, 144407 (2005).
[21] Y. Nakatani, A. Thivillé, and J. Miltat, Nat. Mater. **2**, 521 (2003).
[22] D. Goll, G. Schütz, and H. Kronmüller, Phys. Rev. B **67**, 094414 (2003).
[23] A. Vansteenkiste, M. Weigand, M. Curcic, H. Stoll, G. Schütz, and B. Van Waeyenberge, New J. Phys. **11**, 063006 (2009).
[24] H. Min, R. D. McMichael, J. Miltat, and M. D. Stiles, Phys. Rev. B **83**, 064411 (2011).
[25] NIST Micromagnetic Modeling Activity Group.
[26] S. Hankemeier, A. Kobs, R. Frömter, and H. P. Oepen, Phys. Rev. B **82**, 064414 (2010).
[27] M. J. Donahue and D. G. Porter, "*OOMMF User's Guide, Version 1.0," NISTIR 6376, National Institute of Standards and Technology*, Gaithersburg, MD (Sept. 1999).
[28] W. H. Press, B. P. Flannery, S. A. Teukolsky, and W. T. Vetterling, *Numerical Recipes: The Art of Scientific Computing* (Cambridge University Press, Cambridge, UK, 1986), pp. 515–520.